Int. J. Multiphase Flow Vol. 12, No. 6, pp. 913–933, 1986
Printed in Great Britain.

0301-9322/86 $3.00 + 0.00

MODELLING OF TWO-PHASE TRANSIENT FLOW AND COMBUSTION OF GRANULAR PROPELLANTS

N. C. MARKATOS†

Centre for Numerical Modelling and Process Analysis, Thames Polytechnic, London SE18 6PF, England

(*Received* 10 *January* 1982; *in revised form* 23 *July* 1986)

Abstract—Gas-permeable solid propellants possess great potential for producing high thrusts during extremely short time intervals. The paper presents a theoretical model describing the important physical phenomena taking place in both gaseous and solid phases in such two-phase, unsteady, reactive-flow systems. The governing equations were derived in the form of coupled, non-linear partial differential equations and the resulting formulation was compared with those used by previous authors. A stable, fast-converging, fully-implicit numerical method, first proposed by Spalding and implemented in a general-purpose computer program, was used to solve the equations, so that effects of importance can be studied. Solutions are presented that predict the pressure wave build-up and accelerating flame front for beds of granulated solid propellants fixed in a rigid enclosure, and in gun barrels with an accelerating projectile. The results show that the flame front accelerates and the rate of pressurization increases substantially in the downstream direction. Some discussion is given of the sensitivity of these predictions to the assumed constitutive relations for interphase heat and momentum transfer and the solid burning-rate law. It is argued that the controversy surrounding the hyperbolicity of the equations, which has delayed progress towards theoretical prediction of two-phase flows, is ill-founded, since the equations are shown to possess unique solutions, as indeed do the physical systems they represent.

1. INTRODUCTION

1.1. The Problem Considered and Its Practical Relevance

The present study is concerned with the prediction of the transient phenomena following ignition of granular propellants. The following transient phenomena occur in a few milliseconds: penetration of hot gases into the voids, convective heating of granules to ignition, granule compaction and rapid pressurization. The mass generated in the ignition region accelerates the flame forward, with the region behind the flame rapidly increasing in pressure as more and more mass is being generated. The problem of flame spreading in porous propellant charges is obviously important in the design and analysis of propulsion systems.

In internal ballistics, the initial loading of the solid propellant is an important question. A low initial loading may not impart a final impact strong enough to deliver the shell to a desired distance. On the other hand, a high loading may lead to an uneconomical process owing to the fact that a tightly packed bed would have an inferior surface area to volume ratio to permit complete burning of the propellant. A choice of the optimum initial loading can be achieved only with sufficient quantitative understanding of the physical and chemical processes involved.

Two types of similar problems are considered here; the first involving a chamber with a moving projectile, and the second with rigid boundaries.

1.2. Objectives of the Study

The ability to calculate the transient dynamics resulting from pressure wave formation and flame spreading in a bed of small grain propellant is the motivation for this work. Therefore, the objectives of the study are: (a) to formulate a theoretical model describing the important physical phenomena in question, which allows solutions under all conditions of practical relevance; (b) to solve the associated equations by a stable, fast convergent numerical algorithm; and (c) to demonstrate that results obtained for typical problems are plausible.

The following discussion and results presented refer only to one-dimensional problems.

†Present address: Department of Chemical Engineering, National Technical University, 106 82 Athens, Greece.

1.3. Previous Work and the Present Contribution

The physical and chemical processes taking place in internal ballistics phenomena are complex, and their experimental study is difficult to perform and subject to high degrees of uncertainty and inaccuracy. Due to the above complexities, several theoretical approaches have been proposed.

The theoretical methods can be classified into four categories: (1) statistical models (Buyevich 1971, 1972a, b); (2) continuum-mechanics models (Krier *et al.* 1974, 1976); (3) formal averaging models (Gough 1974a); and (4) two-phase fluid-dynamic models (Kuo *et al.* 1973). The advantages and disadvantages of each of the above methods are analysed by Kuo *et al.* (1976), Koo & Kuo (1977) and Krier & Kezerle (1977).

The method employed in this study follows the approach of Spalding (1979a), which is developed by formulating the governing equations on the basis that mass, momentum and energy fluxes are balanced over control volumes occupied by *space-sharing interspersed continua.* According to that concept, distinct phases are present within the same space (although never at precisely the same time), their shares of space being measured by their "volume fractions".

The resulting differential equations differ from those of previous authors in several respects. In particular:

(a) The gas pressure gradient term is included in the solid-phase momentum equation. Hughes (1976) has argued that such a term results in the mechanical set being non-hyperbolic. Krier & Kezerle (1977) adopted that argument and, in order to obtain solutions to the equations, found it necessary to neglect the above term. However, the present work proves that stable and meaningful results can be obtained when solving the full equations.

(b) The pressure gradient term is written as the partial gradient of pressure and not as the gradient of a partial pressure.

(c) A solid-phase energy equation is used, symmetric with the gas-phase energy equation, instead of the common approach of solving the unsteady heat conduction equation for the solid particle and monitoring the heat gained from the gas in the form of convective heat transfer (Gough 1974a; Kuo *et al.* 1976). The latter approached was not deemed acceptable for the present work, for the reasons discussed by Krier & Kezerle (1977).

A fully-implicit finite-difference scheme was employed for the numerical solutions, with none of the time-step limitations imposed by the explicit methods used by previous authors (Krier & Kezerle 1977).

The predictions for the rigid enclosure problem made by the present model are found to be in fair agreement with the predictions of Krier & Kezerle (1977) for similar conditions. There are no predictions available in the literature for the moving-shell problem.

2. THEORETICAL MODEL

2.1. The Physical Problem

The basic features of the gun barrel are outlined in figure 1. A cylindrical domain is considered, enclosed by the gun barrel and the base of the projectile, and containing a solid propellant in powder form and a gas. The solid propellant comes in various shapes and sizes. In the past, propellants in cord form were in favour. The present-day propellants are still cord-shaped but with slotted tubes. However, spherical forms cannot be ruled out (Koo & Kuo 1977), and this is the form assumed in this study.

Ignition is provided by inflow of hot gas at the base of the cylinder. The gas is forced into the granular bed through a multiply-perforated nozzle, causes a compaction of the granular bed near the entrance region and also heats up the nearby granular propellants to ignition. The so-ignited propellants give off more hot gases which are pushed forward

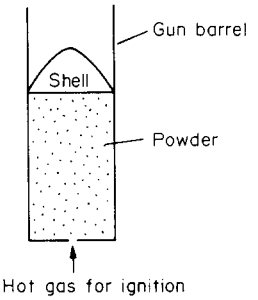

Figure 1. Schematic drawing of a gun barrel.

by the pressure gradient to ignite more propellants. Thus, a steep pressure gradient is created inside the combustion chamber and the accelerated gaseous products cause the shell to move.

2.2. The Dependent and Independent Variables

The following are the dependent variables of the problem:

- gas and particle velocities;
- pressure;
- particle and gas concentrations;
- particle and gas enthalpies.

The independent variables are:

- the distance measured along the barrel, y;
- the time, t.

2.3. The Partial Differential Equations

The equations are derived by considering the balance of fluxes over a control volume small enough to give the desired spatial distributions in the complete system, yet large enough to contain many solid particles, so that the averaged particle velocity and volume fraction are meaningful. The control volume, at any particular time, can be regarded as containing a volume fraction r_i of the ith phase, so that if there are n phases altogether,

$$\sum_{i=1}^{n} r_i = 1. \qquad [1]$$

Each phase is treated as a continuum in the control volume under consideration. The phases "share" the control volume, and they may, as they move within it, interpenetrate.

In the following presentation of the differential equations, the dependent variables will be denoted by lower case letters for the gaseous phase and upper case for the solid phase. For variables other than the main dependent variables (e.g. density), the notation is subscript 1 for the gaseous phase and subscript 2 for the solid phase.

In summary, the important assumptions upon which this flow model is based are listed below:

(1) the two phases are assumed interdispersed and coupled by appropriate interaction terms;
(2) each phase is a continuum, so that derivatives are uniquely defined;
(3) when combustion of particles causes mass transfer between the phases, the solid phase always loses mass while the gas phase gains it;
(4) all gases obey the non-ideal Noble–Abel equation of state with a variable co-volume;
(5) heat transfer to the particles due to radiation is neglected;
(6) the density of the solid phase is constant;

(7) viscous effects other than interphase friction are negligible;
(8) the specific heats are assumed constant.

Except for the first two, these assumptions are made only for simplicity, and by no means represent limitations of the model.

(*a*) *The mass-conservation equations*

Gas-phase mass equation

$$\frac{\partial}{\partial t}(\rho_1 r) + \frac{\partial}{\partial y}(\rho_1 r v) = \dot{m}'''_{21}; \tag{2}$$

Particle-phase mass equation

$$\frac{\partial}{\partial t}(\rho_2 R) + \frac{\partial}{\partial y}(\rho_2 R V) = -\dot{m}'''_{21}; \tag{3}$$

where

r, R = volumetric fractions of gas and solid, respectively,

ρ_1, ρ_2 = density of gas and solid,

v, V = velocity of gas and solid

and

$\dot{m}'''_{21}$ = rate of mass transfer per unit volume from the solid to the gaseous phase.

The volumetric fractions are related by

$$r + R = 1. \tag{4}$$

(*b*) *The conservation of momentum equations*

Gas-phase momentum equation

$$\frac{\partial}{\partial t}(\rho_1 r v) + \frac{\partial}{\partial y}(\rho_1 r v^2) = -r\frac{\partial p}{\partial y} - f(v - V) + \dot{m}'''_{21} V - F_{1w}; \tag{5}$$

Particle-phase momentum equation

$$\frac{\partial}{\partial t}(\rho_2 R V) + \frac{\partial}{\partial y}(\rho_2 R V^2) = -R\frac{\partial p}{\partial y} - (V - v)f - R\frac{\partial \tau}{\partial y} - F_{2w} - \dot{m}'''_{21} V; \tag{6}$$

where

p = the pressure which is regarded as being "shared" between the phases,

f = the interphase friction factor

τ = the intergranular stress.

and

F_{1w}, F_{2w} = friction forces acting on the gas and particles, respectively, by the gun-barrel wall.

The formulation of the pressure terms has occasioned some uncertainty among writers on this subject; and it is sometimes thought that different pressures ought to be provided for each phase. It is not especially useful to do so; therefore, a single pressure appears in *both* equations, and an additional "intergranular force" term in *one* of the equations. This term arises from the "particle-packing" equation, governing the pressure in the solid phase as its volume fraction approaches the physically attainable limit:

$$P = p + \tau\{R\}; \tag{7}$$

wherein the solid phase sustains the extra stress τ, this being a function of the volume fraction, R, to be defined in the next section.

Further inspection of the above equations reveals that the term $p\,\partial r/\partial y$, which frequently occurs in the literature, is missing. This is because use of $\partial/\partial y\,(rp)$ instead of $r\,\partial p/\partial y$ is simply erroneous. A term like $p\,\partial r/\partial y$ implies the presence of a momentum source *proportional to pressure* whenever r is non-uniform. There is no physical mechanism which can produce it. A change in the general *pressure level* would alter such a source; so p would no longer be a relative variable.

Finally, the partial gradient of gas pressure is included in the solid-phase momentum equation. Hughes (1976) has argued that this term results in a non-hyperbolic system and that one might experience difficulties in numerical integration. Krier & Kezerle (1977) reported that stable and well-behaved results were never really achieved when this term was included; pressure and velocity oscillations usually occurred, similar to the problem reported by Dimitstein (1976) and Krier *et al.* (1976). Using the present solution algorithm, first proposed by Spalding (1976), such problems were never encountered; stable and well-behaved results were achieved for all circumstances, even with very coarse mesh sizes.

(*c*) *The conservation of energy equations*

Let $\tilde{h}$, $\tilde{H}$ stand for the stagnation enthalpy of the gas and solid phases per unit mass, respectively, by which is meant the thermodynamic enthalpy plus the kinetic energy of the phase plus any potential energy associated with the position of the fluid in a force field. Then, the first law of thermodynamics leads to the following equations:

Gas-phase energy equation

$$\frac{\partial\,[(\rho_1\tilde{h}-p)r]}{\partial t}+\frac{\partial}{\partial y}\,(\rho_1 rv\tilde{h})=f(v-V)V-H_{11}-\dot{q}_{12}+\dot{m}'''_{21}\left(h_s+\frac{V^2}{2}\right)-\dot{Q}_{1w}; \qquad [8]$$

Particle-phase energy equation

$$\frac{\partial}{\partial t}\,[(\rho_2\tilde{H}-P)R]+\frac{\partial}{\partial y}\,(\rho_2 RV\tilde{H})=f(V-v)v-H_{22}+\dot{q}_{12}-\dot{m}'''_{21}\left(h_s+\frac{V^2}{2}\right)-\dot{Q}_{2w}; \qquad [9]$$

where

$h_s=\tilde{H}+h_c$,

h_c = the heat of combustion of the solid particles,

H_{11}, H_{22} = the rate of heat transfer within the gas and solid phase, respectively, e.g. by conduction and viscous action,

$\dot{q}_{12}$ = heat loss to particles per unit time

and

Q_{1w}, Q_{2w} = the rate of heat loss of the gas and solid phase, respectively, to the gun-barrel wall per unit volume.

For the present study, only the first, third and fourth terms on the r.h.s. of [8] and [9] were included, the rest were assumed to be negligible by comparison.

Other investigators [e.g. Kuo and his co-workers (Kuo & Summerfield 1974; Kuo *et al.* 1976) and Gough (1974b)] did not use a particle-phase energy equation. Instead, they calculated the particle surface temperature by analysing the unsteady heat conduction in the solid phase. Kuo & Summerfield (1974) have made comments in defence of not writing a particle-phase energy equation. It is, however, questionable what mixture energy is being conserved when one does not write such an equation in a form symmetrical to the gas-phase energy equation as done here, and by Gulick (1975), Krier & Kezerle (1977) and Gokhale & Krier (1982).

(d) The particle-size calculation

For the problems under consideration it is necessary to calculate the distribution throughout the field of the average local size of the particles. This necessity arises because, for example, the rate of burning depends strongly upon the size of the particles; and this size diminishes, of course, as the particles are consumed. A complete treatment of the problem involves treating the flow as a multiphase one, the particles being divided into subgroups characterized by having particle sizes lying between prescribed values; and, if so desired, each subgroup can be treated as having its own temperature and velocity. Such an analysis involves much computation, and is necessarily expensive.

The approach followed instead, permits the average particle size to be computed by introducing a second solid volume fraction, R^*, that is the volume fraction which the solid phase would have possessed at each point, in the absence of combustion; the velocities, however, being the same as the phase actually possesses. Therefore R^*, obeys the following equation:

$$\frac{\partial}{\partial t}(\rho_2 R^*) + \frac{\partial}{\partial y}(\rho_2 R^* V) = 0. \qquad [10]$$

The particle size is deduced from

$$\frac{s}{s_0} = \left(\frac{R}{R^*}\right)^{\frac{1}{3}}, \qquad [11]$$

where s stands for some linear dimension of the particle, and s_0 is the value of s for the particles initially. Knowledge of s then permits the local values of the interphase heat-transfer coefficient, interphase friction coefficient and mass-transfer rate to be determined.

Equations [2], [3], [5], [6], [8]–[10] form a system of coupled, non-linear, inhomogeneous partial differential equations.

2.4. Constitutive Relations

The above set of differential equations has to be solved in conjunction with observance of constraints on the values of the variables, represented by algebraic relations. These relations express physical laws of various kinds, governing the critical rate and interaction processes. These constitutive relations follow, in the form used for the present study. It should be mentioned that, although little emphasis is placed on these relations in the context of this paper, their proper form and function are essential for the realistic prediction of the two-phase flows under consideration. A detailed discussion on this subject is given in the original work of Gokhale & Krier (1982).

2.4.1. Equations of state

The Noble–Abel dense-gas law, also called the Clausius equation,

$$p\left(\frac{1}{\rho_1} - b\right) = \bar{\mathrm{R}} T_1, \qquad [12]$$

is used as the equation of state for the gas phase, where $\bar{\mathrm{R}}$ is the specific gas constant ($286.69\ \mathrm{J\,kg^{-1}\,K^{-1}}$) and b is the co-volume which is a function of gas density. For the reported results, b is taken as constant.

The statement of a constant density for the solid particles serves as the equation of state for the particles.

2.4.2. The intergranular stress

Propellant particles cannot be packed so closely as to occupy the whole of space ($R = 1$); instead, an intergranular stress arises which is transmitted through the packed granular

particles and keeps the particles apart. This is like a "pressure" which affects the propellant particles only. The above effect is handled by replacing the $\partial p/\partial y$ term in the particle-phase momentum equation by $\partial(p+\tau)/\partial y$, where τ is the intergranular stress. The constitutive law used for the stress calculation is

$$\tau = 0 \quad \text{for} \quad 0 \leqslant R \leqslant R_{\text{crit}}$$

and [13]

$$\tau = K(R - R_{\text{crit}})^n \quad \text{for} \quad R_{\text{crit}} < R,$$

where R_{crit} is a "critical" volumetric fraction, above which there is no direct contact between particles, and K is a constant representing the rate of change of stresses with respect to R, known from the properties and shape of the particles. In the present study, use is made of the value $n = 1$, i.e. the stresses are taken as a linear function of $(R - R_{\text{crit}})$. Of course, any other value of n could have been used equally well.

2.4.3. The interphase friction coefficient

Prescribed functions for the coefficient in the drag terms of [5] and [6] are used. The expression for the interphase friction force used for a control cell is a linear one,

$$F = \tfrac{1}{2} f \rho_1 |v - V| \frac{A_s}{rR} \qquad [14]$$

where f is an interphase friction parameter and A_s is the area of interphase contact,

$$A_s = \frac{6R}{D_P} \qquad [15]$$

where D_P is the average diameter of the particles.

This simple method was chosen, in view of the lack of reliable empirical correlations, because of its economy and convenience, and is by no means a limitation of the model. For example, the commonly used Ergun (1952) correlation, has very limited application to the combustion of granular propellants under high convective burning situations.

2.4.4. The particle burning rate

For the burning law, a simple, empirical pressure-dependent relation was employed, namely

$$\dot{b} = \epsilon \left(\frac{p}{p_{\text{atm}}}\right)^n, \qquad [16]$$

where p_{atm} is the atmospheric pressure and ϵ and n are constants.

The production rate of gases from solid particles, $\dot{m}_{21}$, is therefore given by

$$\dot{m}_{21} = R\rho_2 \dot{b} \left[\frac{S}{V}\right]_P = \frac{R\rho_2 \dot{b}}{\frac{D_P}{6}}, \qquad [17]$$

where $[S/V]_P$ is the surface area/volume ratio for a single particle.

2.4.5. Ignition criterion

The criterion for particle ignition used in this study assumes ignition to have occurred when the surface temperature of a particle reaches a critical value, e.g.

$$\dot{b} = 0 \quad \text{for} \quad T_s < T_{\text{ign}}$$

and

$$\dot{b} = \epsilon \left(\frac{p}{p_{\text{atm}}}\right)^n \quad \text{for} \quad T_s \geqslant T_{\text{ign}}. \qquad [18]$$

The surface temperature of the particles is determined by assuming a cubic temperature profile within the particle, as outlined below.

2.4.6. The interphase heat-transfer coefficients

Although the equations solved for the transport of heat between the gas and particle phases are those of the phase enthalpies [8] and [9], it is convenient to think in terms of temperatures T_1 and T_2, by introduction of the specific heats C_1 and C_2.

Central to the following treatment is the concept of an interface between the two phases, with temperature T_s.

Inspection of [8] and [9] reveals that the following quantities need be calculated, since they appear as source/sink terms in the above phase-enthalpy equations: $\dot{q}_{1s}$, the heat input to the surface from phase 1; $\dot{q}_{s2}$, the heat flow from the surface to phase 2 (solid particles); and $\dot{m}_{21}$, the mass transferred from phase 2 to phase 1. These quantities are related to the various temperatures by the following relations:

$$\dot{q}_{1s} = a_1(T_1 - T_s), \tag{19}$$

$$\dot{q}_{s2} = a_2(T_s - T_2) \tag{20}$$

and

$$\dot{m}_{21} = 0 \quad \text{for} \quad T_s < T_{ign}$$

and

$$\dot{m}_{21} = f\{p\} \quad \text{for} \quad T_s \geqslant T_{ign}, \tag{21}$$

where the "interface transfer parameters", a_1 and a_2, are heat-transfer coefficients multiplied by the interface area through which the transfer occurs, and $f\{p\}$ is the function given by [18] above.

An energy balance over a control volume enclosing the interface yields:

Heat coming into the control volume $= \dot{q}_{1s} + \dot{m}_{21}C_2T_2$,
heat going out of the control volume $= \dot{q}_{s2} + \dot{m}_{21}C_2T_s$

and

generation $= \dot{m}_{21}h_c$.

Therefore

$$\dot{q}_{s2} - \dot{q}_{1s} = \dot{m}_{21}[h_c - C_2(T_s - T_2)]. \tag{22}$$

Combination of [19], [20] and [22] yields

$$T_s = \frac{1}{\zeta}[a_2T_2 + a_1T_1 + \dot{m}_{21}(h_c + C_2T_2)], \tag{23}$$

$$\dot{q}_{1s} = \frac{a_1}{\zeta}[a_2(T_1 - T_2) + \dot{m}_{21}C_2(T_1 - T_2) - \dot{m}_{21}h_c] \tag{24}$$

and

$$\dot{q}_{s2} = \frac{a_2}{\zeta}[a_1(T_1 - T_2) + \dot{m}_{21}h_c], \tag{25}$$

where

$$\zeta = a_1 + a_2 + \dot{m}_{21}C_2. \tag{26}$$

The particle surface temperature, T_s, is crucial in determining when ignition occurs, according to [21] above. Its determination is made difficult by the fact that the heating of the particles by the hot gases does not penetrate far into the particle since the transient interval of the physical process is only a few milliseconds. Therefore, the temperature profile inside the particle has a very steep gradient and the particle surface reaches the ignition condition long before the thermal wave penetrates to the centre of the particle; or, in other words, T_s may change substantially whilst the bulk particle temperature, T_2, changes very little.

The approach used in this study is to determine the coefficient a_2, in [20] for heat transfer from the surface into the particle, from

$$\dot{q}_{s2} = a_2(T_s - T_2) = -\lambda \left.\frac{\partial T}{\partial r}\right|_s, \qquad [27]$$

where λ is the thermal conductivity of the granular material, and the temperature gradient at the surface

$$\left.\frac{\partial T}{\partial r}\right|_s$$

is determined by assuming a cubic temperature profile within the particle.

The outcome of some lengthy algebra is the following relation:

$$a_2 = \frac{3\lambda}{\delta} = \frac{3\lambda}{\frac{5}{2}R\left[1 - \sqrt{1 - \frac{8}{5}\left(\frac{T_2 - T_\infty}{T_s - T_\infty}\right)}\right]}, \qquad [28]$$

where

R = the radius of the particle,

T_∞ = the initial temperature at its centre, assumed constant,

and

δ = the thermal wave penetration depth in a spherical particle, computed at each time step.

The heat-transfer parameter a_1 is estimated by assuming the Nusselt number equal to 2, which is a very doubtful assumption given the high Reynolds numbers encountered. T_s is then calculated from [23]. A Newton–Raphson iteration is used to derive a_2 from the cubic particle temperature distribution.

Again, as Gokhale & Krier (1982) observe, there is little in the literature that would provide an accurate expression. Such an expression should take into account the "blowing" into the thermal boundary layers adjacent to the particles (Gokhale & Krier 1982).

3. FINITE-DOMAIN EQUATIONS

3.1. The Grid

The finite-domain versions of the governing differential equations given above are derived by integrating the latter over the volume of a cell enclosing a grid node. The grid used in the present work is "staggered" as shown in figure 2, from which it will be seen that the control volume for continuity is different from that for momentum. For the variables r_i and h_i, these control volumes are the ones centred on grid nodes such as P (in figure 2) and having faces which bisect the lines joining P to N and S at right angles. For the velocity components the control volumes are like those just described; but they are displayed in the direction y by distances which place the relevant velocity locations at their centres. The practice is conventional (Kurosaki & Spalding 1979; Patankar & Spalding 1972).

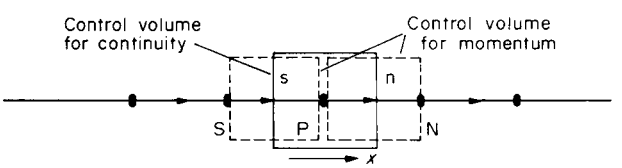

Figure 2. Control volume and grid nodes.

For the case of the moving projectile, the above grid was expanded at every time step, to follow the increase in the y range.

3.2. *The Equations*

The result of integrating the equations is expressed in terms of the values of the variables pertaining to grid points. This is done by way of interpolation rules, which do not significantly differ from those for single-phase prediction procedures (Kurosaki & Spalding 1979; Patankar & Spalding 1972).

The above operations result in a set of algebraic equations which have already been reported by Markatos *et al.* (1978), Spalding (1979a) and Kurosaki & Spalding (1979), and are not presented here.

4. THE SOLUTION PROCEDURE

The task for this problem is to determine sets of values, for all the points of the grid, for all the time instants considered, and for both phases, of: p, r, R, $\tilde{h}$, $\tilde{H}$ at central grid points, and of v, V at velocity grid points. Because of the high degree of non-linearity and interlinkage of the equations, the task must be performed by iterative means. It is therefore necessary to use a reliably convergent successive-adjustment procedure. The procedure used is the IPSA (interphase slip algorithm) procedure of Spalding (1976), which was first applied to the steam–water flow in steam generators (Markatos *et al.* 1978). This is an implicit algorithm which anticipates the effects of a change in the local property of one phase on the properties of the other phase at the same location. An outline of the procedure is provided below. At each time interval, the solution procedure proceeds according to the following steps:

(i) Determine the boundary conditions at the upper and lower boundaries of the y range, for all variables.
(ii) Solve the finite-domain equations for the enthalpies of the two phases individually, by use of the partial-elimination algorithm (Spalding 1979a) (because of the strong linkage between those enthalpies).
(iii) Solve the finite-domain equations for R at all grid points by way of the tridiagonal matrix algorithm (TDMA).
(iv) Obtain the r values from [4].
(v) Determine the pressure distribution which is appropriate to the momentum equations of the two phases, added together. This is a simple forward-integration process along the y-direction.
(vi) Using the pressure distribution, solve for the velocities of the two phases individually by the partial-elimination algorithm.
(vii) Compute the consequent errors in the continuity equation for the two phases added together, and so formulate the "pressure-correction" equation.
(viii) Solve for the pressure corrections by TDMA and apply to the velocities the resulting corrections, proportional to pressure-correction differences.
(ix) Return to step (ii), and repeat the cycle of computations until the continuity errors computed at step (viii) are sufficiently small.
(x) Proceed to the next time interval, and start the cycle of operations again from step (i).

More details may be found in Markatos *et al.* (1978), Spalding (1979a, b) and Markatos & Kirkcaldy (1983).

This procedure was found to converge satisfactorily for the problems under consideration, over a wide range of conditions. Use was made of a general computer program, PHOENICS (Spalding 1981; Rosten & Spalding 1986), that implements the above procedure, while allowing the user to perform easily his own particular modelling.

5. RESULTS

5.1. Introduction

The cases considered in the present work fall into the following two classes:

(i) two-phase combustion in a rigid enclosure (i.e. fixed grid); and
(ii) two-phase combustion in a gun barrel with an accelerating projectile (i.e. expanding grid).

Extensive studies on the variations of the parameters involved (e.g. constants in the burning-law, intergranular stress and interphase drag constitutive expressions) were carried out. For all the computations performed, convergence was fast and monotonic. The results presented here correspond to those values of the parameters, which appeared to be the most realistic during the parametric studies.

Table 1 summarizes the input used to carry out the typical results shown below, including initial conditions, for the rigid enclosure problem. The data used for this problem correspond closely to those of Krier & Kezerle (1977).

Table 2 presents the same information for the accelerating projectile problem. The probjectile velocity and acceleration were calculated, at every time step, from the computed force acting on its base. Both problems are specified after a time, chosen as $t = 0$, in which at one end of the domain an ignition stimulus is assumed by specifying a region of high pressure, hot gases. This "ignition" region was taken to be about 2.5% of the total domain length. The heat transfer from the hot gases to the particles raises the particle surface temperature, until the ignition temperature is reached, initiating combustion.

The main results presented are the pressure distribution as time progresses, the gas and particle velocities, the gas volume fraction and the temperature histories of both phases.

5.2. Computational Details

The presented results are the outcome of careful grid and time-step independence tests.

Table 1. Input data used in the numerical computations for the rigid-enclosure problem

Parameter	Value
Geometry	
Gas-space length, L	0.0762 m
Physical properties	
Density of gas, ρ_1	$1.124\ \mathrm{kg\,m^{-3}}$
Density of propellant particles, ρ_2	$1580.55\ \mathrm{kg\,m^{-3}}$
Specific heat ratio of gas, γ	1.252
Specific gas constant, $\bar{\mathrm{R}}$	$286.69\ \mathrm{J\,kg^{-1}\,K^{-1}}$
Ignition temperature, T_{ign}	350 K
Chemical energy released, h_c	$5.49 \times 10^6\ \mathrm{J\,kg^{-1}}$
Specific heat of gas, C_1	$1000\ \mathrm{J\,kg^{-1}\,K^{-1}}$
Specific heat of propellant particles, C_2	$1467.6\ \mathrm{J\,kg^{-1}\,K^{-1}}$
Thermal conductivity of solid particles	$0.2243\ \mathrm{kg\,m\,s^{-3}\,K^{-1}}$
Constitutive relations	
Co-volume of gas, b	$1.0784 \times 10^{-3}\ \mathrm{m^3\,kg^{-1}}$
Propellant burning-rate proportionally constant, ϵ	10^4
Propellant burning-rate index, n	1.0
Intergranular stress proportionality constant, K	10^9
Intergranular stress index, n	1.0
Interphase friction parameter, f	10^6
Interphase heat-transfer parameter on the gas side, a_1	10^3
Critical volume fraction, R_{crit}	0.6
Initial conditions	
Pressure, p	$10^5\ \mathrm{N\,m^{-2}}$
Bulk temperature of solid particles, T_2	300 K
Temperature at the centre of a particle, T_x	298 K
Temperature of gas, T_1	300 K
Temperature of igniting gas at the lower end of the domain	3300 K
Pressure of igniting gas	$1.065 \times 10^6\ \mathrm{Nm^{-2}}$
Volume fraction of solid, R	0.6
Velocities of gas and particles, v, V	0.0
Initial average particle diameter	4.12×10^{-4} m

Table 2. Input data used in the numerical computations for the accelerating projectile problem

Parameter	Value
Geometry	
Gas-space length at time 0, L	0.2 m
Physical properties	
Density of gas, ρ_1	$1.124\ \mathrm{kg\,m^{-3}}$
Density of propellant particles, ρ_2	$1000\ \mathrm{kg\,m^{-3}}$
Specific heat ratio of gas, γ	1.4
Specific gas constant, $\bar{R}$	$286.69\ \mathrm{J\,kg^{-1}\,K^{-1}}$
Ignition temperature, T_{ign}	350 K
Chemical energy released, h_c	$5.49 \times 10^6\ \mathrm{J\,kg^{-1}}$
Specific heat of gas, C_1	$1000\ \mathrm{J\,kg^{-1}\,K^{-1}}$
Specific heat of propellant particles, C_2	$1467.6\ \mathrm{J\,kg^{-1}\,K^{-1}}$
Thermal conductivity of solid particles λ	$0.2243\ \mathrm{kg\,m\,s^{-3}\,K^{-1}}$
Constitutive relations	
Co-volume of gas, b	$1.0784 \times 10^{-3}\ \mathrm{m^3\,kg^{-1}}$
Propellant burning-rate proportionality constant, ϵ	10^4
Propellant burning rate index, n	1.0
Intergranular stress proportionality constant, K	10^9
Intergranular stress index, n	1.0
Interphase friction parameter, f	10^6
Interphase heat-transfer parameter on the gas side, a_1	10^3
Critical volume fraction, R_{crit}	0.5
Initial conditions	
Pressure, p	$10^5\ \mathrm{N\,m^{-2}}$
Bulk temperature of solid particles, T_2	300 K
Temperature at the centre of a particle, T_α	298 K
Temperature of gas, T_1	300 K
Temperature of igniting gas at the lower end of the domain	3300 K
Pressure of igniting gas	$1.065 \times 10^6\ \mathrm{N\,m^{-2}}$
Volume fraction of solid, R	0.5
Velocities of gas and particles, v, V	0.0
Initial average particle diameter	4.12×10^{-4} m
Other input	
Mass of projectile (used in calculating its acceleration from the pressure difference at its base and the atmospheric)	5 kg

It was found that grids consisting of 42 or more control cells gave nearly identical results, and the same was true for time steps of 7×10^{-7} s or less. A grid of 42 control cells and a time step of 7×10^{-7} s was therefore chosen to carry out the typical results shown below.

The CPU time taken is 6.87×10^{-3} s per grid node/per sweep/per time step/per main variable, on a Perkin–Elmer 3220 minicomputer. This time is equivalent to 4.29×10^{-4} s on an IBM 30/32 system. Typically, 10 sweeps were required to obtain full convergence at each time step. Therefore, a full run simulating a transient of 200 time steps, and using the 42 control cells grid, requires about 4 min CPU time on an IBM 30/32 system.

The above times include of course the computation of the auxiliary variables: τ, ρ, $\dot{m}_{21}$ and T_s.

5.3. Results for the Rigid-enclosure Problem

Figures 3–10 present the distribution histories of the fluid-dynamic and heat-transfer variables in a rigid enclosure, 0.0762 m long, with an initial solid loading of 60%. Other pertinent input data to the calculations are indicated in table 1.

Figure 3 outlines the calculated pressure distributions at five different times (39.2, 50.4, 56.0, 64.4 and 70 μs). As in previous work related to this problem (see Krier *et al.* 1977), the appearance of a "continental divide" in the interior of the bed is pronounced. The predictions indicate a rapid build-up of pressure leading to steep pressure gradients, forming a shock-line front. In addition, the average pressures behind the front are very high. A peak pressure of $4.6 \times 10^9\ \mathrm{N\,m^{-2}}$ is predicted at $t = 70\ \mu$s. This is in good agreement with the peak pressure of $4.9 \times 10^9\ \mathrm{N\,m^{-2}}$ (720 kpsia) predicted by Krier & Kezerle (1977) for a similar problem. Furthermore, the overall pressure distribution history predicted by the present method is in good qualitative and quantitative agreement with that of Krier & Kezerle (1977). However, the present distributions lag those of Krier &

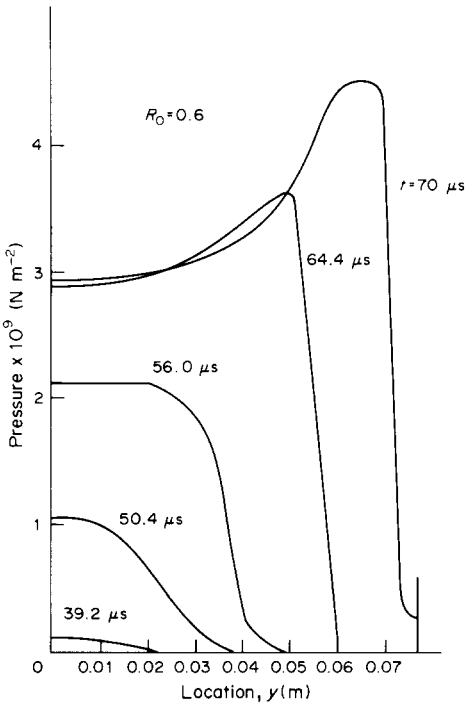

Figure 3. Pressure distribution history for the rigid-enclosure problem.

Kezerle by about 13 μs. A likely explanation is that the initial "ignition stimulus" is imposed over different lengths in the two studies. For the present predictions, the "ignition" region was taken to be about 2.5% of the total chamber length. Krier & Kezerle do not mention their "ignition" region. However, Krier *et al.* (1977) used 15% in a study of a similar problem. This much greater "ignition region" would explain the observed time lag.

During the above pressure build-up, the ignition front accelerates moderately at first and then more rapidly, as shown in figure 4, which presents the locus of that front. The front accelerates from a speed (slope of the y–t locus) of 0.7–1.39 mm μs^{-1} after about 37 μs and to 2 mm μs^{-1} after about 60 μs. This is to be compared with 0.83 mm μs^{-1} around $t = 20$ μs and 1.97 mm μs^{-1} around $t = 50$ μs, predicted by Krier & Kezerle (1977). Also shown in this figure is the locus of the peak pressure. For the small initially ignited portion of the bed, the flame front accelerates slowly into the bed, while for some time (around 35 μs) the peak presure remains at the ignited end, near $y = 0$. However, at around

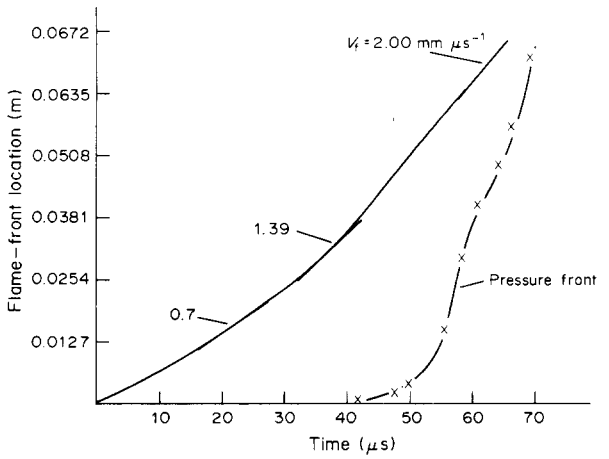

Figure 4. Flame-front and pressure-front loci for the pressure distributions indicated in figure 3.

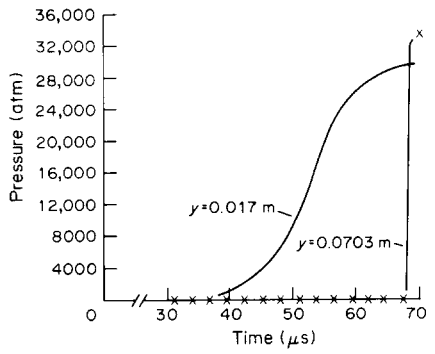

Figure 5. Predicted pressure–time traces at $y = 0.017$ m and $y = 0.0703$ m.

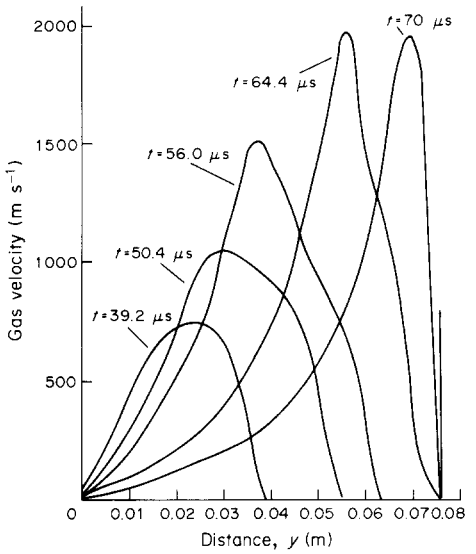

Figure 6. Gas velocity distribution history.

40 μs in time, the pressure front begins to move into the bed and accelerates rapidly towards the ignition front. Should the pressure front precede the flame front, then detonation would start. This did not occur within the time interval studied herein.

Figure 5 presents the predicted values of pressure–time traces at an upstream location, $y = 0.0117$ m, and a downstream one, $y = 0.0703$ m. The pressurization process at the downstream portion lags that at the upstream but it increases faster and eventually overtakes the upstream pressure trace. This is consistent with experimental data obtained from pressure transducers for similar test situations, as reported by Koo & Kuo (1977).

Figures 6 and 7 show the gas velocity and the propellant-particle velocity distributions at the chosen times. As might be expected, a peak develops in the velocity profile driven by the pressure gradient, which develops as a consequence of the steep pressure front arriving at the various locations. Also worth noting are the extreme gas velocities, often exceeding 1500 m s^{-1}, and the fact that peaks in particle velocity lag behind peaks in gas velocity at any given time. The particle velocities are in general lower than the gas velocity, since the inertia of the particles is greater than that of gas. Comparison of figures 6 and

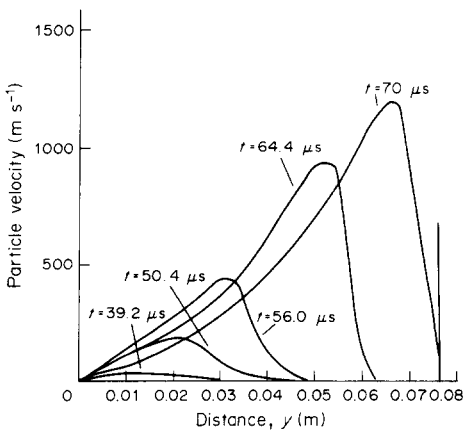

Figure 7. Particle velocity distribution history.

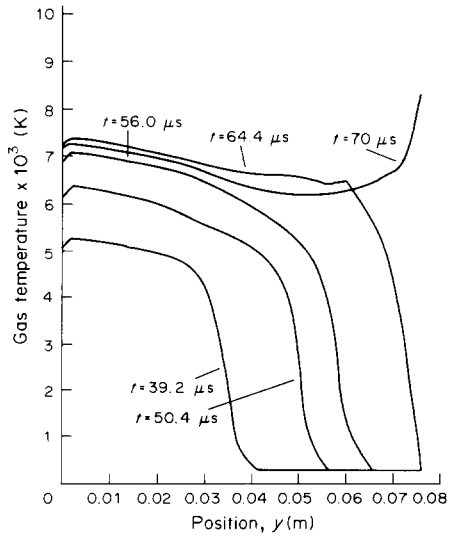

Figure 8. Gas temperature distribution history.

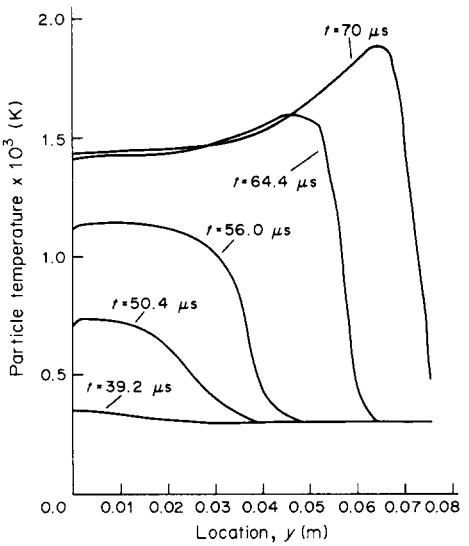

Figure 9. Particle temperature distribution history.

7 with the corresponding figures of Krier & Kezerle (1977) reveals that there is good qualitative and quantitative agreement. For example, the predicted maximum gas velocity is 1970 m s^{-1}, compared with the 2100 m s^{-1} of Krier & Kezerle. However, the present distributions lag behind the distributions of Krier & Kezerle by about 13 μs, which is consistent with the time lag observed in the pressure distribution, explained above.

Figures 8 and 9 present gas and particle temperature distribution histories. Due to combusion, the gas temperatures are generated at very high values (>6000 K). These temperatures decay as the gas loses heat to the solid by convection into the bed interior. Later, as the pressure front steepens, the gas is compressed to values (~8000 K) exceeding their values at the lower part of the domain. The steady increase in the particle temperature is due to convective heat transfer. Comparison of figures 8 and 9 with those of Krier & Kezerle reveals that there are differences in the two sets of results, particularly in that the present particle temperature distribution peaks abruptly after about $t = 64.6\,\mu$s, near the top of the chamber, a feature which appears in Krier & Kezerle's results near the bottom of the chamber at $t = 100.6\,\mu$s. [figure 4.15 of Krier & Kezerle (1977)]. The unrealistically high gas temperatures are due to assumptions 4 and 8 in section 2.3, which preclude the flow of energy into dissociation of the gaseous combustion products. The rather large particle temperatures predicted at later times are a consequence of the surface/volume ratio increasing inversely with particle diameter, as the particles burn out. Therefore, the particle temperature predictions are spurious as $r \to 1.0$, since there are no particles left; but then its value does not influence the convective flame spreading significantly.

The final predictions presented for the rigid-enclosure problem are the gas volume-fraction distribution histories shown in figure 10. The gas volume-fraction profiles show that near the lower end of the enclosure the porosity increases fairly rapidly. This is due to both a reduction in volume of the particles due to burning and the forward motion of these particles being carried along by the gas. Subsequently, the forward drag on the particles results in their compaction further downstream, to loadings greater than the original 60%. The present distributions are in good qualitative and quantitative agreement with those of Krier & Kezerle (1977), and they lag them by about 13 μs, which is consistent with the time lag previously discussed.

5.4. Results for the Accelerating Projectile Problem

Figures 11–19 present the distribution histories of the fluid-dynamic and heat-transfer variables in a gun barrel 0.2 m long, with an initial solid loading of 50%. Other pertinent input data to the calculations are indicated in table 2.

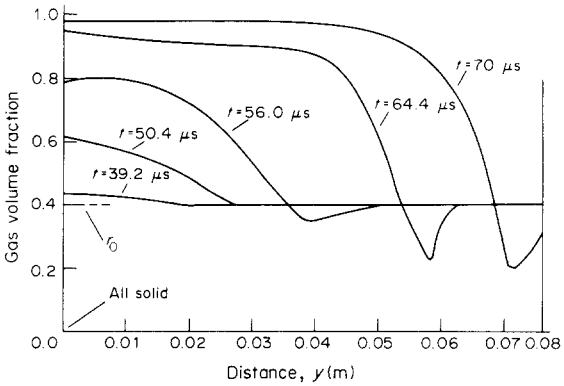

Figure 10. Gas volume-fraction distribution history.

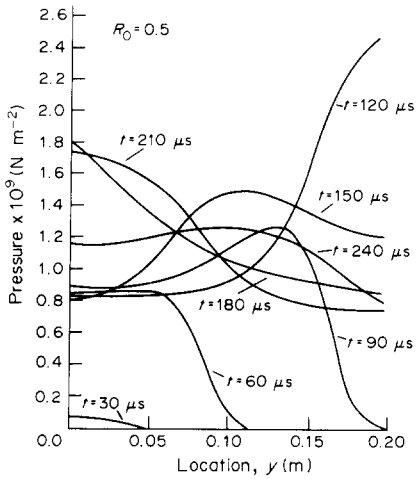

Figure 11. Pressure distribution history for the accelerating projectile problem.

Figure 11 presents the calculated pressure distributions at five different times (30, 60, 90, 120 and 150 μs). Beginning with the trace $t = 30\ \mu$s, the predictions indicate a build-up of pressure leading to steep pressure gradients which become steeper with increasing time, from the increased gasification rate. At $t = 120\ \mu$s, the pressure achieves an overall maximum of about 2.5×10^9 N m^{-2}, and subsequently a steep pressure reversal is predicted

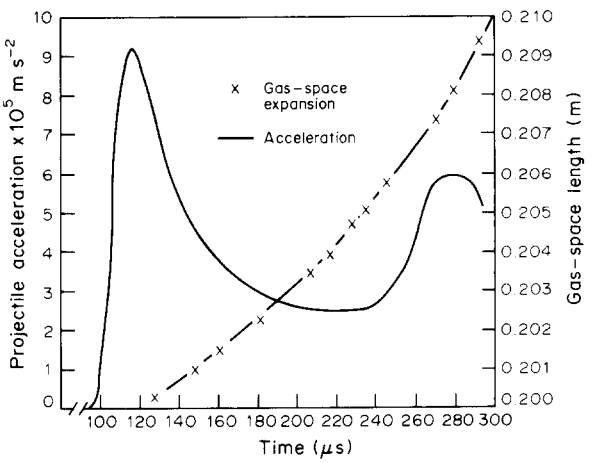

Figure 12. Projectile acceleration and gas-space expansion history.

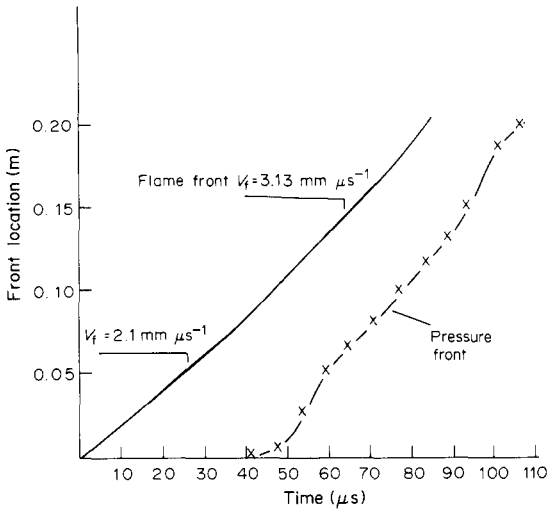

Figure 13. Flame-front and pressure-front loci for the pressure distributions indicated in figure 11.

after the pressure front strikes the base of the projectile, when nearly all particles have been consumed. The pressure level then decreases as the projectile moves forward, and the gas space increases. A new pressure reversal is predicted after the pressure front strikes the lower end of the gun barrel at about $t = 180\,\mu$s, and a pressure peak strikes again the base of the projectile at around $t = 280\,\mu$s. This pressure peak is this time lower than before at about $1.75 \times 10^9\,\mathrm{N\,m^{-2}}$. The above pressure behaviour agrees qualitatively with observations behind projectiles, and is reflected in the projectile acceleration variations which are indicated in figure 12, together with the rate of domain expansion.

During the above pressure build-up, the ignition front accelerates from a speed of about 2.1–3.13 mm μs^{-1} after about 66 s (figure 13). Also shown in figure 13 is the locus of the peak pressure. For the small initially ignited portion of the bed, the flame front accelerates into the bed, while for some time (around 42 μs) the peak pressure remains at the ignited end, near $y = 0$.

After $t = 42\,\mu$s, the pressure front moves into the bed and accelerates towards the ignition front with a speed of around 3.13 mm μs^{-1}, i.e. at the same speed as the final flame front, indicating that there will not be a cross-over of the two fronts.

Figure 14 presents the predicted pressure–time traces at an upstream location, $y = 0.025$ m, and a downstream one, $y = 0.175$ m. The pressurization process at the downstream portion again lags behind that at the upstream; but it increases much faster, overtaking the upstream trace.

Figures 15 and 16 show the gas velocity and the particle velocity distributions at four chosen times, up to 120 μs, when nearly all particles are consumed. Again, a peak develops in the velocity profile driven by the pressure gradient, and peaks in particle velocity lag behind peaks in gas velocity at any given time. Worth noting is the negative gas velocity at the top of the barrel at $t = 120\,\mu$s. This reverse flow of gas causes the pressure trace of $t = 120\,\mu$s to cross that of $t = 90\,\mu$s.

Figures 17 and 18 show the temperature distributions for gas and particles. Due to combustion, the gas temperatures are generated at very high values ($\sim$6000 K). These temperatures decay as the gas loses heat to the solid by convection into the bed interior. Later as the peak pressure is reached, and the particles are nearly all consumed, the gas is compressed to values ($\sim$7500 K) exceeding their values at the lower end of the gun barrel.

The increase in the particle temperature is due to convective heat transfer. The same comments given in the previous section for the unrealistically high temperatures apply here also.

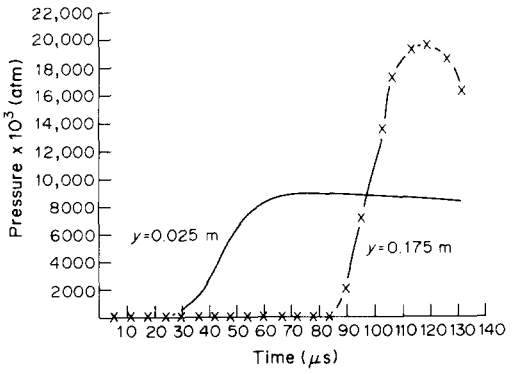

Figure 14. Predicted pressure–time traces at $y = 0.025$ m and $y = 0.175$ m.

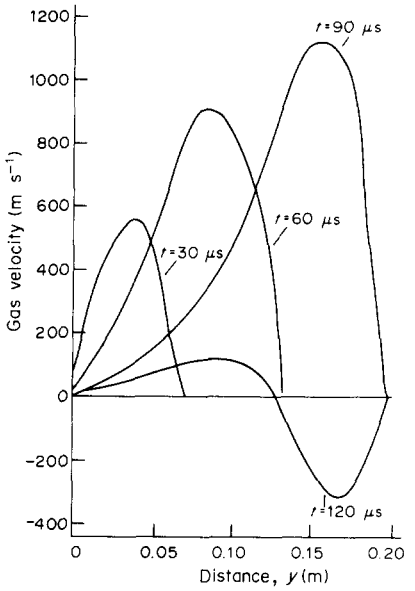

Figure 15. Gas velocity distribution history.

The final predictions presented for the accelerating projectile problem are the gas volume-fraction distribution histories shown in figure 19. The gas volume-fraction profiles show that, near the lower end of the gun barrel, the porosity increases rapidly. This is again due to both a reduction in volume of the particles due to burning and the forward motion of these particles. No compaction of particles to loadings greater than the original 50% is observed, and this is a difference between the rigid enclosure and the accelerating projectile results. Nearly all particles have been consumed by around $t = 120\,\mu$s.

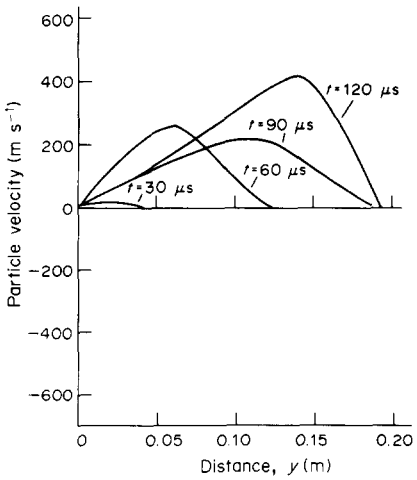

Figure 16. Particle velocity distribution history.

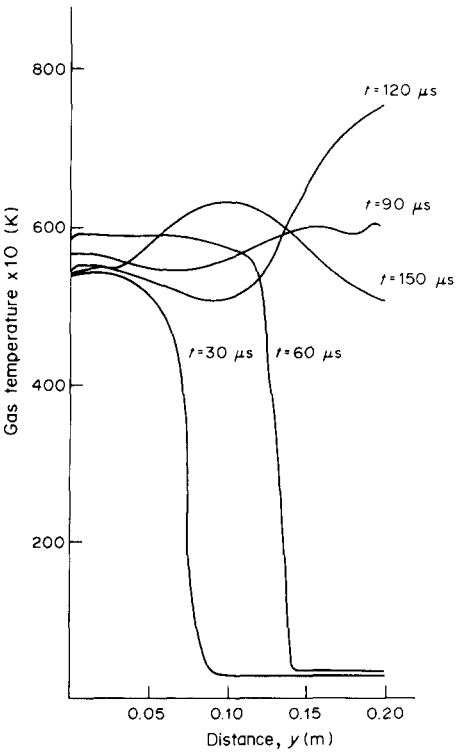

Figure 17. Gas temperature distribution history.

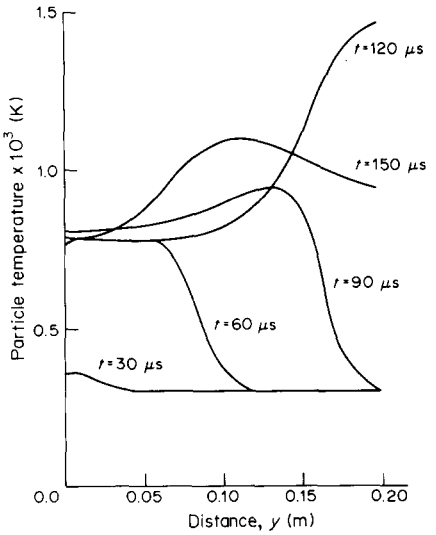

Figure 18. Particle temperature distribution history.

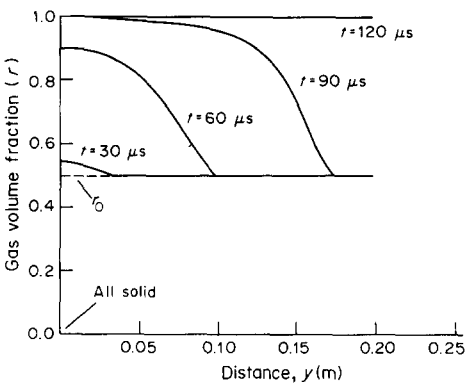

Figure 19. Gas volume-fraction distribution history.

6. CONCLUSIONS

A self-consistent theoretical model is described for the combusion of mobile granular propellants. A stable, fast-converging numerical scheme is used for solving the complete system of equations. It is found unnecessary to eliminate terms from the equations in order to obtain meaningful results. No numerical instability was experienced over a wide range of applications, thus no artificial smoothing was necessary. It appears therefore that the stability problems experienced by previous workers were due to the solution schemes used rather than any intricacies in the equations set.

A computer code, PHOENICS, incorporating the theoretical model, has been applied for the computation of two typical cases of two-phase phenomena occurring in gun barrels. The results are shown to be physically plausible. The transient wave phenomena and flame spreading are predicted well by the model, which indicates that the rate of pressurization increases in the downstream direction and the pressure peak developed travels downstream, as expected.

The model is general and applicable also to two- and three-dimensional problems. Work for such cases has already been reported (Markatos & Kirckaldy 1983). It is concluded that the mathematical formulation of the gun-barrel two-phase flow considered is a satisfactory one, and that the solution procedure is a reliable and economical one. There are no known problems associated with the mathematical model. The remaining problems are associated with the physical processes of the two-phase flows, namely the heat, mass and momentum transfer between the phases (Gokhale & Krier 1982). More work is required to review the literature for reliable experimental correlations on the above processes and to establish their effects on the model predictions. Indeed, much more work is required experimentally in establishing those experimental correlations. New hypotheses are needed, guided by experimental observations. Numerical computations of the present kind can effect these comparisons.

Acknowledgements—This paper is based on work conducted under contract from Société Nationale de Poudres et Explosifs (SNPE), France. The author acknowledges with thanks the valuable comments and criticisms offered by Miss C. Kuche and Mr M. Dervaux of SNPE. Thanks are also due to CHAM Ltd, London, for permitting the use of their code PHOENICS.

REFERENCES

BUYEVICH, Y. A. 1971 Statistical hydromechanics of disperse systems—1: physical background and general equations. *J. Fluid Mech.* **49**(3), 498–507.

BUYEVICH, Y. A. 1972a Statistical hydromechanics of disperse systems—2: solution of the kinetic equation for suspended particles. *J. Fluid Mech.* **52**(2), 345–355.

BUYEVICH, Y. A. 1972b Statistical hydromechanics of disperse systems—3: pseudo-turbulent structure of homogeneous suspensions. *J. Fluid Mech.* **56**(2), 313–336.

DIMITSTEIN, M. 1976 A separated-flow model for predicting the pressure dynamics of highly loaded beds of granulated propellant. MSE Thesis, Aero/Astro Engineering Dept, Univ. of Illinois at Urbana Champaign, Ill.

ERGUN, S. 1952 Fluid flow through columns. *Chem. Engng Process* **48,** 89–96.

GOKHALE, S. S. & KRIER, H. 1982 Modelling of unsteady, two-phase reactive flow in porous beds of propellant. *Prog. Energy Combust. Sci.* **8,** 1–39.

GOUGH, P. S. 1974a Fundamental investigation of the interior ballistics of guns. Final Report IHCR 74-1, Naval Ordnance Station, Indian Head, Md.

GOUGH, P. S. 1974b Fundamental investigation of the interior ballistics of guns. Report SRC-R-74, Space Corp, Md.

GULICK, F. E. C. 1975 Conservation equations for a reacting two-phase flow based on continuum theory. Summary notes for *Wkshp 12th JANNAF Combustion Mtg*, Newport, R.I.

HUGHES, E. D. 1976 Field balance equations for two-phase flows in porous media. In *Proc. Two-phase Flow and Heat Transfer Symp. 1976*, Univ. of Miami, Fla (Edited by VEZIROGLU T. N.).

KOO, J. H. & KUO, K. K. 1977 Transient combustion in granular propellant beds. Report BRL CR 346, Dept of Mechanical Engineering, Pennsylvania State Univ., Philadelphia, Pa.

KRIER, H. & KEZERLE, J. A. 1977 Modelling of convective mode combustion through granulated propellant to predict transition to detonation. Technical Report AAE77-17 (UILU-Eng 77 0517), Aero/Astro Engineering Dept, Univ. of Illinois at Urbana Champaign, Ill. Presented at *17th Symp. (Int.) on Combustion*, The Combustion Institute, Pittsburgh, Pa (1979).

KRIER, H. & RAJAN, S. 1975 Flame spreading and combustion in packed beds of propellant grains. *AIAA 13th Aerospace Sciences Mtg*, Pasadena, Calif., Paper No. 75-240. Also: *AIAA Jl* **14**(3), 301–309 (1976).

KRIER, H., VAN TASSEL, W. F., RAJAN, S. & VERSHAW, J. T. 1974 Model of gun propellant flame spreading and combustion. Report BRL CR 147, Ballistic Research Lab., Aberdeen Proving Ground, Md. Also published as: VAN TASSEL, W. F. & KRIER, H. 1975 *Int. J. Heat Mass Transfer* **18,** 1377–1386.

KRIER, H., DIMITSTEIN, M. & GOKHALE, S. S. 1976 Reactive two-phase flow models applied to the prediction of detonation transition in granulated solid propellant. Technical Report AAE76-3 (UILU-Eng 76-0503), Aero/Astro Engineering Dept, Univ. of Illinois at Urbana Champaign, Ill.

KRIER, H., GOKHALE, S. S. & HUGHES, E. D. 1977 Modelling of convective mode combustion through granulated solid propellant to predict possible detonation transition. *AIAA/SAE 13th Propulsion Conf.*, Paper No. 77-857.

KUO, K. K. & SUMMERFIELD, M. 1974 High-speed combustion of mobile granular solid propellants. *15th Symp. on Combustion*, Combustion Institute, Pittsburgh, Pa, pp. 515–525.

KUO, K. K., VICHNEVETSKY, R. & SUMMERFIELD, M. 1973 Theory of flame front propagation in porous propellant charges under confinement. *AIAA Jl* **11**(4), 444–451.

KUO, K. K., KOO, J. H., DAVID, T. R. & COATES, G. R. 1976 Transient combustion of mobile gas-permeable propellants. *Acta Astronaut.* **3,** 573–591.

KUROSAKI, Y. & SPALDING, D. B. 1979 One-dimensional unsteady two-phase flows with

interphase slip: a numerical study. Presented at *2nd Multiphase Flow and Heat Transfer Symp. Wkshp*, Miami Beach, Fla.

MARKATOS, N. C. & KIRKCALDY, D. 1983 Analysis and computation of 3D, transient flow and combustion through granulated propellants. *Int. J. Heat Mass Transfer* **26,** 1037–1053.

MARKATOS, N. C., MOULT, A., PHELPS, P. J. & SPALDING, D. B. 1978 The calculation of steady three-dimensional two-phase flow and heat transfer in steam generators. *Proc. ICHMT Semin. 1978*, Dubrovnik, Yugoslavia, pp. 485–502. Hemisphere, Washington, D.C.

PATANKAR, S. V. & SPALDING, D. B. 1972 A calculation procedure for heat, mass and momentum transfer in three-dimensional parabolic flows. *Int. J. Heat Mass Transfer* **15,** 1797–1806.

ROSTEN, H. I. & SPALDING, D. B. 1986 *PHOENICS—Beginners Guide and Users Manual.* CHAM TR/100, London.

SPALDING, D. B. 1976 The calculation of free-convection phenomena in gas–liquid mixtures. *Proc. ICHMT Semin.*, Dubrovnik, Yugoslavia p. 569. Hemisphere, Washington, D.C.

SPALDING, D. B. 1979a Numerical computation of multi-phase fluid flow and heat transfer. In *Recent Advances in Numerical Methods in Fluids*, Vol. 1 (Edited by TAYLOR, C. and MORGAN, K.). Pineridge Press, Swansea.

SPALDING, D. B. 1979b Numerical computation of multi-phase flows. (NCMPF) A lecture course at Purdue University, W. Lafayette, Ind.

SPALDING, D. B. 1981 A general purpose computer program for multidimensional one- and two-phase flow. *Maths Comput. Simuln* **XXIII,** 267–276.